

The Precision and Accuracy of AIRS Level 1B Radiances for Climate Studies

Thomas Hearty^a, Steve Gaiser^a, Tom Pagano^a, Hartmut Aumann^a

^aJet Propulsion Laboratory/California Institute of Technology, 4800 Oak Grove Drive,
Pasadena, USA;

ABSTRACT

We investigate uncertainties in the Atmospheric Infrared Sounder (AIRS) radiances based on in-flight and pre-flight calibration algorithms and observations. The global coverage and spectral resolution ($\lambda/\Delta\lambda \sim 1200$) of AIRS enable it to produce a data set that can be used as a climate data record over the lifetime of the instrument. Therefore, we examine the effects of the uncertainties in the calibration and the detector stability on future climate studies. The uncertainties of the parameters that go into the AIRS radiometric calibration are propagated to estimate the accuracy of the radiances and any climate data record created from AIRS measurements. The calculated radiance uncertainties are consistent with observations. Algorithm enhancements may be able to reduce the radiance uncertainties by as much as 7%. We find that the orbital variation of the gain contributes a brightness temperature bias of < 0.01 K. Although this can be removed by algorithm enhancements, it is smaller than uncertainty of the gain for most channels.

Keywords: AIRS, Climate, Calibration

1. INTRODUCTION

The components of the noise in the AIRS gain and radiance are analyzed by accounting for all of the parameters that go into the gain and radiance equations. Section 2 describes the equations used in the AIRS Level 1B radiance calculations. Section 3 describes the error propagation equations used in this analysis. Section 4 describes the periodicities seen in some parameters. Section 5 describes the components to the uncertainty in the AIRS gains. Section 6 describes the components to the uncertainty in the AIRS radiances. Section 7 describes the conclusions of this analysis.

We also examine the radiance uncertainties of three granules (i.e., 6 minutes of AIRS data) from June 20th, 2003 with very different scene characteristics to understand how the radiance errors depend on the scene and orbital characteristics:

1. Granule 119: Daytime Sahara
2. Granule 130: Antarctica
3. Granule 217: Daytime Equatorial Pacific.

2. THE RADIANCE AND GAIN EQUATIONS

The radiance of each channel in the AIRS infrared spectra of Earth is determined from the following equation:

$$N_{sc,i,j} = \frac{a_{0,i,j} + \bar{a}_1(dn_{i,j} - dn_{off,i}) + a_2(dn_{i,j} - dn_{off,i})^2}{1 + p_r p_t \cos[2(\theta_j - \delta)]} \quad (1)$$

where all parameters but θ_j are functions of frequency,

$a_{0,i,j}$ = an offset applied because of the scan mirror (see Equation. 3).

\bar{a}_1 = the mean gain for the granule (`gain_stats.mean`).

Further author information: (Send correspondence to T.H.)

T.H: E-mail: Thomas.J.Hearty@jpl.nasa.gov, Telephone: 1 818 354 2762

$dn_{i,j}$ = the counts for the jth footprint of the ith scan.

$dn_{off,i}$ = the detector offset for scan i calculated as described in the LIB Requirements document.

a_2 = second order coefficient obtained from pre-flight testing.

$p_r p_t$ = the product of the emissivity of the scan mirror, the polarization factor of the scan mirror, and the polarization factor of the spectrometer determined from pre-flight testing.

θ_j = is the scan angle of the jth footprint.

δ = the phase of the polarization of the AIRS spectrometer determined from pre-flight testing. This is currently 0 for all channels. The denominator of the radiance equation is neglected for the analysis.

The gain is calculated for each scan and then averaged over the 135 scans in a granule. The gain for scan i in units of radiance per count is calculated from the following equation:

$$a_{1,i} = \frac{N_{obc,i}(1 + p_r p_t \cos 2\delta) - a_{0,i}(\theta_{obc}) - a_2(dn_{obc,i} - dn_{off,i})^2}{dn_{obc,i} - dn_{off,i}} \quad (2)$$

where,

$N_{obc,i}$ = Radiance of the on-board calibration (obc) blackbody source for scan i calculated as described in the LIB Requirements document from telemetry and the Planck blackbody equation.

$a_{0,i}$ = the correction for the scan angle dependence at the angle of the obc.

$\theta_{obc} = \pi$.

$dn_{obc,i}$ = counts measured from the obc source in scan i.

An offset is applied to the gain due to thermal emission from the scan mirror.

$$a_{0,i,j} = N_{m,i} \times p_r p_t \times [\cos 2(\theta_j - \delta) + \cos 2\delta] \quad (3)$$

where,

$N_{m,i}$ = Radiance of a unit emissivity surface at the scan mirror temperature obtained from the telemetry and the Planck blackbody equation.

3. ERROR COMPONENTS

3.1. Error Propagation Equations

This analysis makes use of the standard error propagation equations and neglects the off diagonal components of the covariance matrix. The uncertainty in a given quantity, X, is denoted by ΔX . In some cases the uncertainty is approximated by the standard deviation of that parameter, while in other cases it is inferred in other ways.

The uncertainty in the gain is derived from its components using the following equation:

$$(\Delta \bar{a}_1)^2 = \sum_{i=1}^{135} \left[\left(\frac{\partial \bar{a}_1}{\partial dn_{obc,i}} \right)^2 (\Delta dn_{obc})^2 + \left(\frac{\partial \bar{a}_1}{\partial dn_{off,i}} \right)^2 (\Delta dn_{off})^2 + \left(\frac{\partial \bar{a}_1}{\partial T_{obc,i}} \right)^2 (\Delta T_{obc})^2 + \left(\frac{\partial \bar{a}_1}{\partial T_{sm,i}} \right)^2 (\Delta T_{sm})^2 \right] \quad (4)$$

Similarly the error of the radiance is calculated from its components using the following equation:

$$(\Delta N_{i,j})^2 = \left(\frac{\partial N_{i,j}}{\partial dn_{sc}} \right)^2 (\Delta dn_{sc})^2 \dots$$

$$+ \sum_{k=1}^{135} \left[\left(\frac{\partial N_{i,j}}{\partial dn_{obc,k}} \right)^2 (\Delta dn_{obc})^2 + \left(\frac{\partial N_{i,j}}{\partial dn_{off,k}} \right)^2 (\Delta dn_{off})^2 + \left(\frac{\partial N_{i,j}}{\partial T_{obc,k}} \right)^2 (\Delta T_{obc})^2 + \left(\frac{\partial N_{i,j}}{\partial T_{sm,k}} \right)^2 (\Delta T_{sm})^2 \right] \quad (5)$$

The values used for the errors in the counts (Δdn_{sc} , Δdn_{obc} , Δdn_{sv}) are derived in Section 3.2. The error in the temperatures (ΔT_{obc} and ΔT_{sm}) are taken from the LIB parameters that report the standard deviation of these temperatures, `input_bb_temp.dev` and `input_scan_mirror_temp.dev`, respectively. Since these temperatures do show some time variability (see, Section 4) these estimates of their uncertainty are probably overestimated. Nevertheless, their contributions to the total gain and radiance uncertainty is negligible.

Another way of looking at the total error of the radiance is to treat the gain as an independent parameter. Then the radiance error propagation equation can be written as follows:

$$(\Delta N_{i,j})^2 = \left(\frac{\partial N_{i,j}}{\partial dn_{i,j}} \right)^2 (\Delta dn_{sc})^2 + \left(\frac{\partial N_{i,j}}{\partial \bar{a}_1} \right)^2 (\Delta \bar{a}_1)^2 + \left(\frac{\partial N_{i,j}}{\partial dn_{off,i}} \right)^2 (\Delta dn_{off})^2 \quad (6)$$

where $\Delta \bar{a}_1 = \frac{\text{gain_stats.dev}}{\sqrt{135}}$.

The components to the radiance uncertainty using both Equation 5 and Equation 6 will be investigated in Section 6. For this analysis we have neglected the error terms due to the uncertainty of the scan mirror emissivity and the OBC emissivity which have been evaluated by preflight measurements^{1,2}

3.2. Error in Counts

The detector offset of the channels in modules M3 through M10 ‘‘droops.’’ The droop is compensated for in these channels by having DC Restores every 20 minutes which clamp the electronics. Because of the droop, the standard deviation of the counts for these channels is larger than the true uncertainty and cannot be used in the error propagation equations described above (see Figure 1). However, the true uncertainty in the counts can be inferred from the standard deviation of the space view signals, ΔS_{sv} , and the standard deviation of the blackbody signals, ΔS_{obc} , which are given by the `input_space_signals.dev` and `input_bb_signals.dev` fields in the limited engineering structures that provide statistics on the signals (i.e., counts – offset) rather than the counts.

The uncertainty in the space view counts (Δdn_{sv}) and the space view offset (Δdn_{off}) can be derived if we assume constant conversion factors between the standard deviation of space view signals and the uncertainty of space view counts:

$$\Delta dn_{sv} = Const_{sv} \times \Delta S_{sv} \quad (7)$$

$$\Delta dn_{off} = Const_{off} \times \Delta S_{sv} \quad (8)$$

We estimated the conversion factors $Const_{sv}$ and $Const_{off}$ can be found by generating a pseudo random distribution of numbers with a mean of zero and standard deviation of one. This distribution was used as a model for the space view counts, $dn_{sv,model}$. An offset, $dn_{off,model}$, was calculated from this distribution using the same algorithm used for the AIRS space view offset calculation. Specifically, the offset for every ‘‘scan’’ was calculated as the median of 8 numbers in the distribution, 4 from the current scan, 2 from the previous scan, and 2 from the following scan. A scan is a set of 4 consecutive numbers in the distribution. A model distribution of space view signals, $S_{sv,model}$, can then be derived by subtracting their corresponding offsets (i.e., $S_{sv,model} = dn_{sv,model} - dn_{off,model}$). The conversion from the standard deviation of space view signals to space view counts is then,

$$Const_{sv} = \frac{\Delta dn_{sv,model}}{\Delta S_{sv,model}} \quad (9)$$

and the conversion from the standard deviation of space view signals to the standard deviation of the space view offset is,

$$Const_{off} = \frac{\Delta dn_{off,model}}{\Delta S_{sv,model}} \quad (10)$$

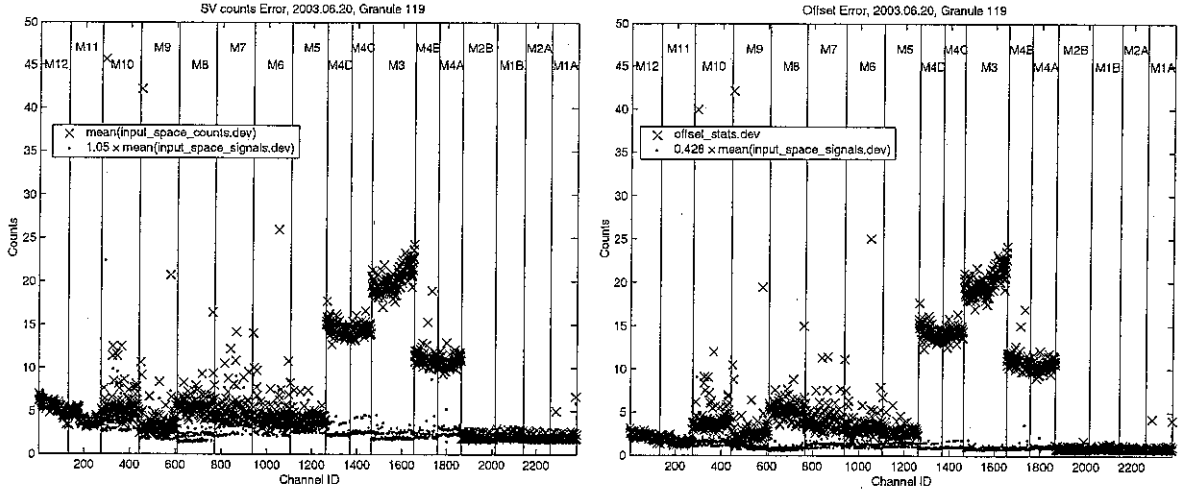


Figure 1. The uncertainty of the space view counts and the space view offset can be approximated using the standard deviation of the space view signals. The apparent bifurcation of the noise in the counts seen in some modules is the result of some channels using the A or B side only and other channels using both the A and the B sides of the detectors. The uncertainty of the obc counts can be approximated using the standard deviation of the obc signals and the standard deviation of the space view signals.

Using an array with 1 million points gives $Const_{sv} = 1.05$ and $Const_{off} = 0.428$. Thus, the uncertainty in the space view counts is $\Delta dn_{sv} = 1.05 \times \text{input_space_signals.dev}$ and the uncertainty in the space view offset is $\Delta dn_{off} = 0.428 \times \text{input_space_signals.dev}$. This can be verified by comparing the model errors with the actual errors for the channels from modules M1A, M1B, M2A, M2B, M11, and M12, that do not have droop (Figure 1).

The uncertainty in the blackbody counts (Δdn_{obc}) can be derived from ΔS_{obc} and Δdn_{off} :

$$\Delta dn_{obc} = \sqrt{(\Delta S_{obc})^2 - (\Delta dn_{off})^2}. \quad (11)$$

where,

$$\Delta S_{obc} = \text{input_bb_signals.dev}.$$

The noise in the scene counts can be inferred from the noise in space view counts and the noise in the obc counts by converting the counts to photons and then assuming they obey Poisson statistics. The number of photons in the space view, n_{sv} , can be derived from the number of counts, dn_{sv} , using the conversion factor A:

$$n_{sv} = A \times dn_{sv}. \quad (12)$$

Thus, if we assume Poisson statistics the following is also true:

$$\Delta n_{sv} = A \times \Delta dn_{sv} = \sqrt{A \times dn_{sv}}. \quad (13)$$

Similar equations apply for the number of photons in the Earth scene, n_{sc} , and the obc view, n_{obc} . Since the signal of the scene is $S_{sc} \sim dn_{sc} - dn_{sv}$ and the signal of the obc is $S_{obc} \sim dn_{obc} - dn_{sv}$, the uncertainty of the scene counts can be expressed as follows:

$$\Delta dn_{sc} = \sqrt{\frac{S_{sc}}{S_{obc}} \times (\Delta dn_{obc}^2 - \Delta dn_{sv}^2) + \Delta dn_{sv}^2}. \quad (14)$$

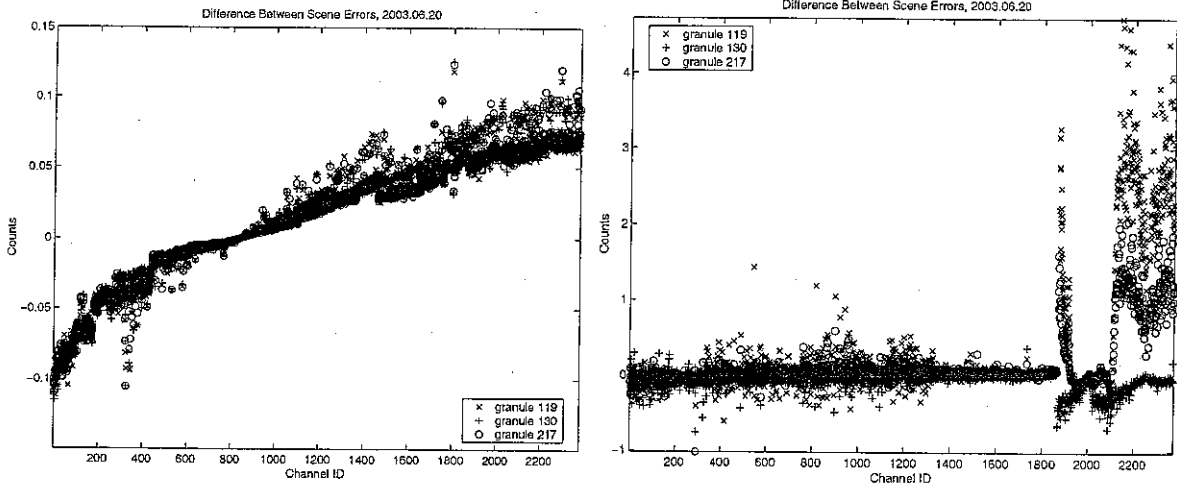


Figure 2. The difference between Δdn_{sc} for a 250 K reference scene using the approximations made here and the approximations made in the PGE are displayed (i.e., $\Delta dn_{sc} - \Delta dn_{sc,pge}$). Both are calculated for a 250 K reference scene. The difference between Δdn_{sc} using the approximations made in this analysis and the approximations made in the PGE (i.e., $\Delta dn_{sc} - \Delta dn_{sc,pge}$). In this case, Δdn_{sc} is calculated using the actual mean signal of the scene and $\Delta dn_{sc,pge}$ is calculated for a 250 K reference scene.

This analysis calculates Δdn_{sv} , Δdn_{obc} , and Δdn_{sc} as described above and makes the following approximation:

$$\frac{S_{sc}}{S_{obc}} = \frac{\text{input_scene_counts.mean} - \text{offset_stats.mean}}{\text{input_bb.signals.mean}} \quad (15)$$

3.3. The PGE Approximations

The Noise Equivalent Radiance (NeN) provided in the Level 1B data product is calculated for a 250 K reference scene using only the scene component from Equation 5 and Equation 6, ignoring the denominator and the second order terms in the radiance equation. Thus,

$$\text{NeN} = |\bar{a}_1| \times \Delta dn_{sc}. \quad (16)$$

The PGE also makes slightly different approximations than are used in this analysis when calculating Δdn_{sc} . Specifically, the PGE makes the following approximations:

$$\Delta dn_{sv} = \text{input_space_signals.dev} \quad (17)$$

$$\Delta dn_{obc} = \text{input_bb.signals.dev} \quad (18)$$

$$\frac{S_{sc}}{S_{obc}} = \frac{N_{sc}}{N_{obc}} \quad (19)$$

where the scene and obc radiances, N_{sc} and N_{obc} , are calculated from the Planck blackbody formula for a 250 K reference scene and the temperature of the on-board calibration source, respectively. The PGE approximations work well for most channels. However, they result in a small channel dependent bias in the magnitude of Δdn_{sc} (Figure 2). Also, the uncertainty in the scene counts can be significantly miscalculated in some channels by using a 250 K reference scene (Figure 2).

The uncertainty in the scene counts for most channels does not depend on the scene. However, the channels in modules M1A, M1B, M2A, and M2B do depend on the scene temperature. Figure 3 displays the absolute errors in the scene counts as they are calculated here and as they are calculated in the PGE for 2 granules

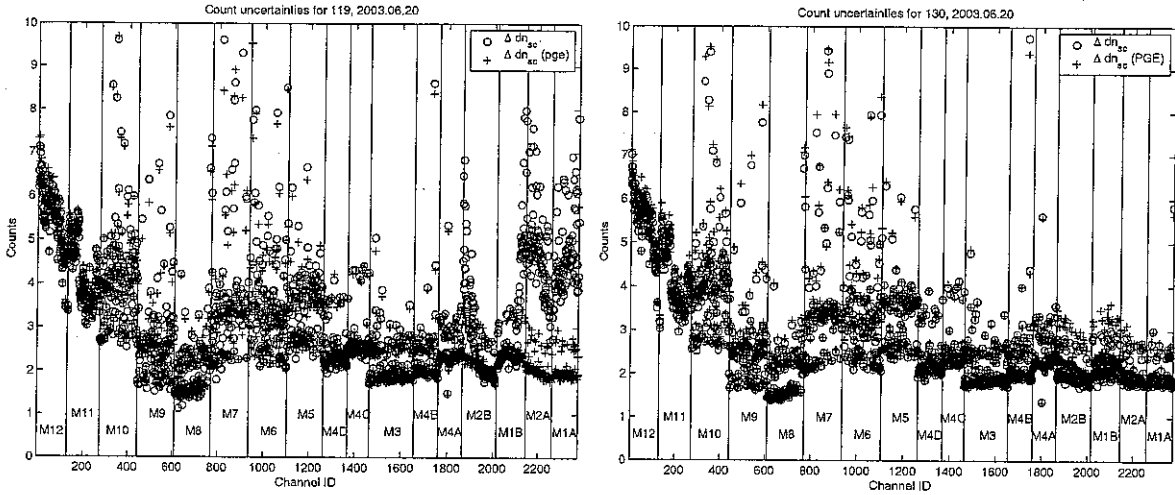


Figure 3. The uncertainties in the scene counts are different than those used in the PGE NeN calculation because the actual scene temperatures were used rather than the 250 K reference temperature.

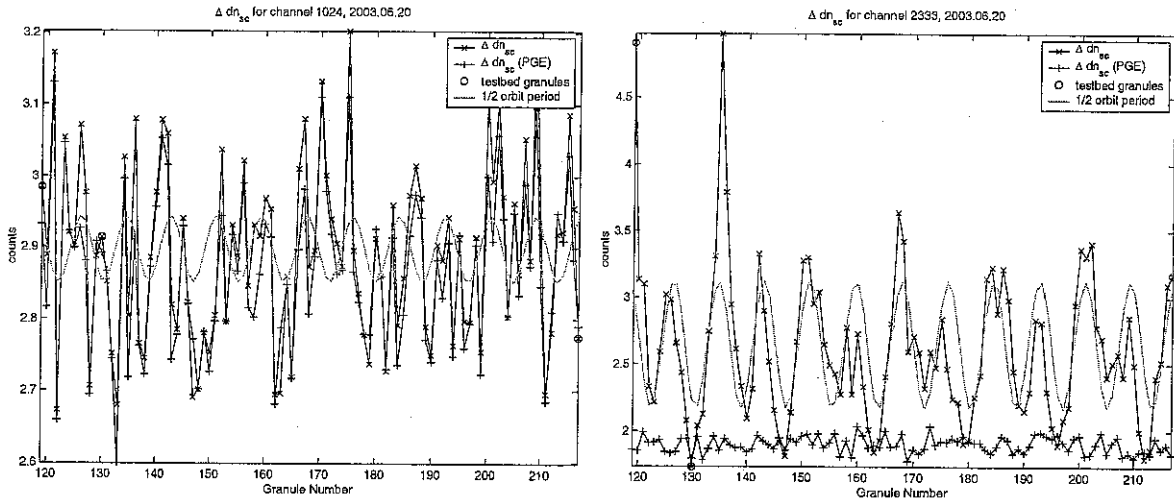


Figure 4. The error in the counts of channel 2333 is sensitive to the scene temperature and the error in the counts of channel 1024 is not sensitive to scene temperature. The 3 granules described in Section 2 are marked with red circles.

with different scene characteristics. Since the temperature can vary dramatically across a scene even within one granule users should be aware that the NeN in the the Level 1B data is calculated for a 250 K reference scene and they should calculate their own NeN for scenes that differ from this using the NeN algorithm described in the Level 1B Requirements document if their needs require a more accurate estimate of the NeN.

Using the algorithm adopted here which uses the average scene signals to calculate the uncertainty, a variation can be seen with a period of half an orbital period for the channels that are sensitive to scene temperature (Figure 4). For most channels there is no significant periodicity in the NeN (or NEdT) as it is calculated in the PGE. However, if the scene is accounted for as described in this document, the channels in Modules 1A, 1B, 2A, and 2B (e.g., channel 2333), which are the most affected by photon noise, do show a significant variability due to the scene temperature.

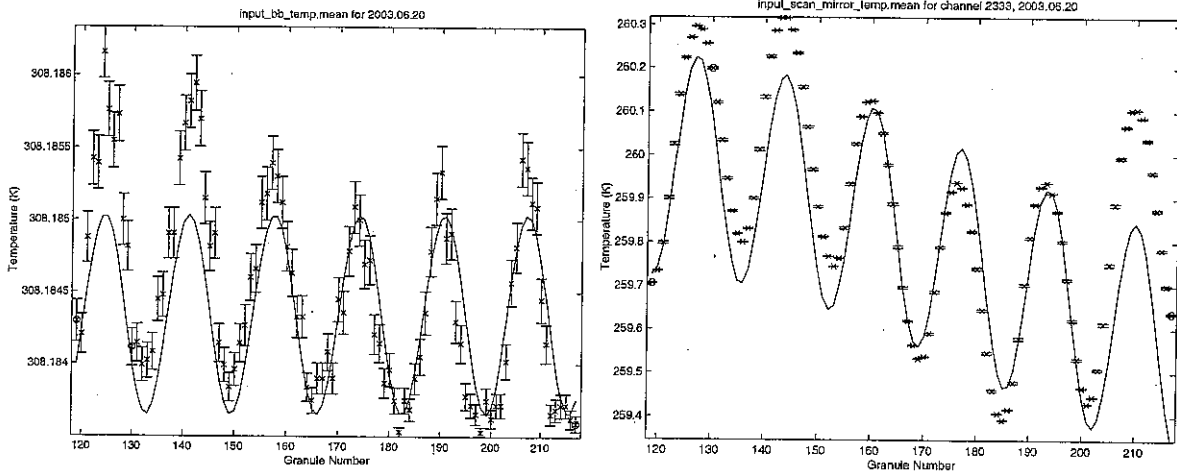


Figure 5. The blackbody temperature shows an orbital periodicity. The scan mirror temperature also shows a sinusoidal orbital periodicity and a daily periodicity that is not well modeled by a sine curve.

4. PERIODICITIES

In addition to the periodicity seen in the uncertainty of the scene counts, many of the parameters used in the AIRS gain and radiance calibration also show an orbital periodicity. The scan mirror temperature shows 2 periodicities, a sinusoidally varying temperature with an orbital period and daily variation. Figure 5 shows the blackbody temperature and the scan mirror temperature for a portion of the day on June 20th.

The space view offset and blackbody counts both show some variability depending on the channel. Figure 6 displays the time series of space view counts, blackbody counts, blackbody signal, and the gain for 2 channels that do not have DC Restores. For some channels the orbital variability is calibrated out when calculating the signal and the gain (e.g., channel 204) and for other channels it is not (e.g., channel 2333).

5. GAIN ERRORS

The error we calculated agrees well with the standard deviation of the gain over the granule suggesting no significant sources of uncertainty have been omitted.

Since the gain can vary sinusoidally with an orbital period of ~ 99.31 minutes and we calculate a mean gain for each 6 minute granule, the gain can have a **maximum** bias of $\sim 0.19 \times A$ (i.e., $\text{maxbias} = A \times \sin[\omega t_{\frac{1}{2}}]$, where $\omega = \frac{2\pi}{99.31}$ minutes $^{-1}$, $t_{\frac{1}{2}} = 3$ minutes, and A is the amplitude of the gain variation). Since the amplitude of the gain variation is small, this error is generally less than the uncertainty in the gain itself. However, although it should average out globally, the error due to the gain variation can produce a radiance bias in one direction at the start of a granule and in the other direction at the end of the granule. Figure 7 displays the total gain uncertainty in temperature units and the maximum bias that can be expected from using the average gain over a granule. Although the bias can be larger than the uncertainty for some channels the absolute temperature bias is small. Figure 7 also shows that for most channels the maximum error in the gain due to the orbital periodicity is less than the uncertainty in the gain. However, for some channels the maximum error due to the periodicity can be roughly equal to or larger than the gain uncertainty.

Figure 8 displays the relative error of each component of the gain uncertainty by dividing each of the contributions by the gain. The main contribution to the uncertainty of the gain is due to the uncertainty in the counts of the obc and to a lesser extent to the uncertainty in the space view offset. The relative error due to the uncertainty of the obc temperature and the scan mirror temperature is negligible compared with the other components.

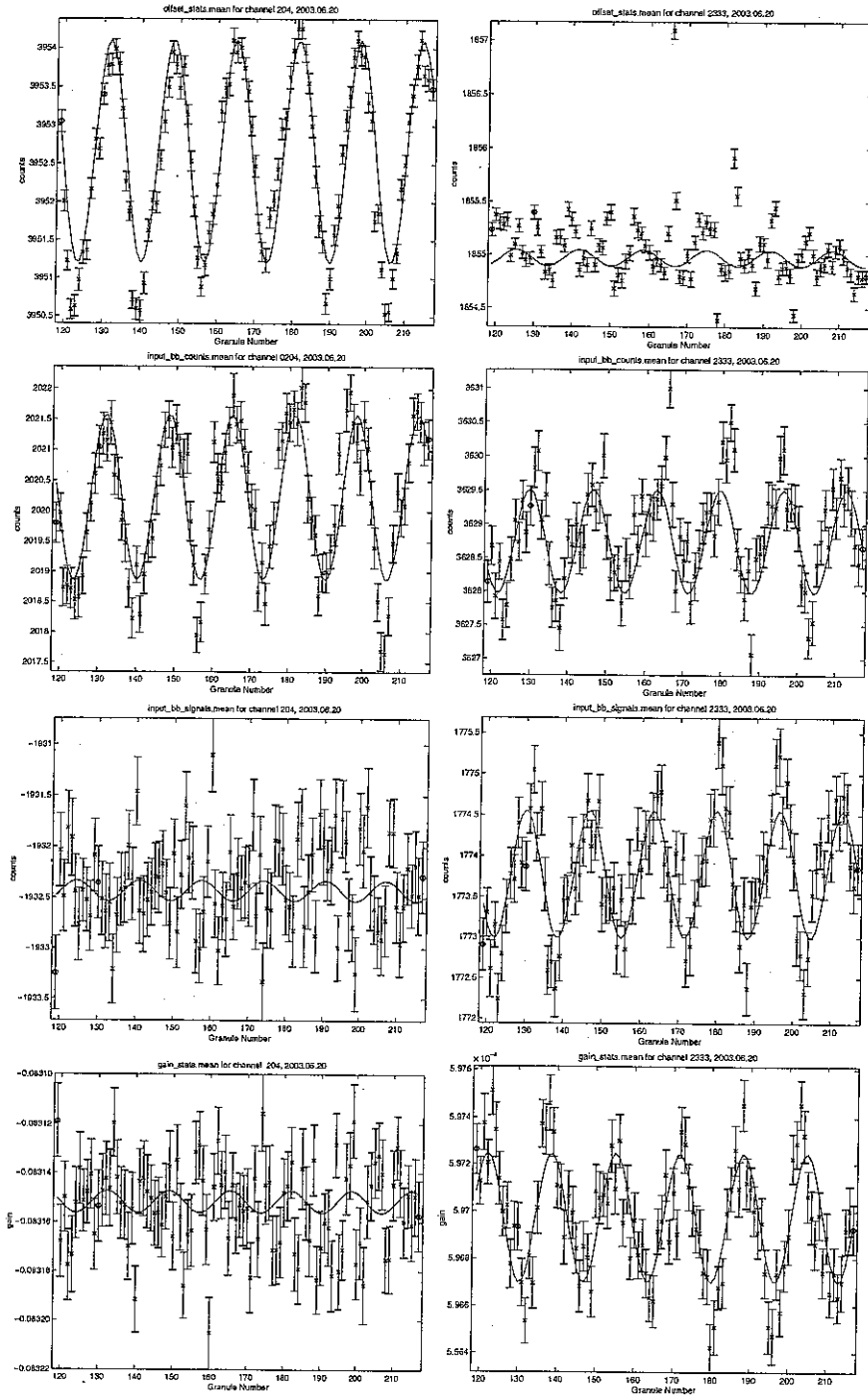


Figure 6. The space view offset, the obc counts, and the obc signals show orbital periodicities. The periodicities seen in the counts is mostly calibrated out of the signal for channel 204, but it is still present in the signal of channel 2333.

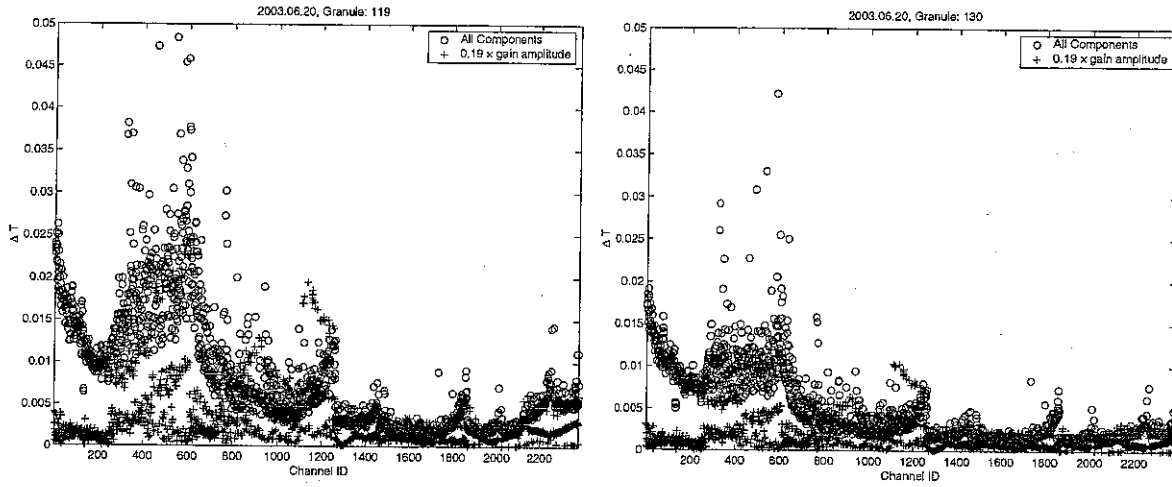


Figure 7. The sum of all the gain error components in temperature units is compared with the maximum error expected from the orbital periodicity. Although the bias is larger than the gain uncertainty for some channels the magnitude of the bias is much smaller than other sources of error that go into the radiance calculation.

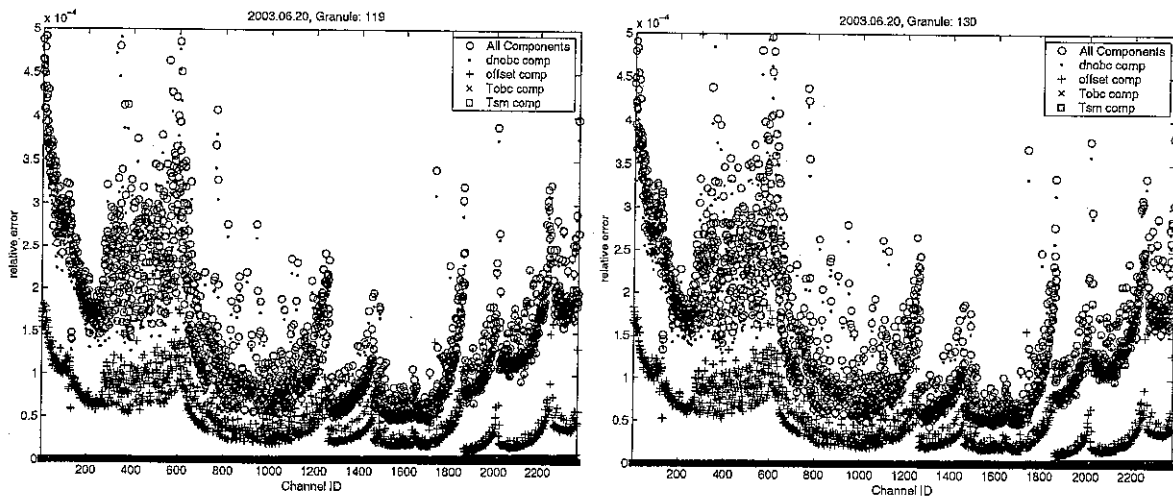


Figure 8. This figure shows the relative error for each of the components to the error of the mean gain (i.e., \bar{a}_1) for 3 granules. The relative error is calculated by dividing each component by the absolute value of the mean gain.

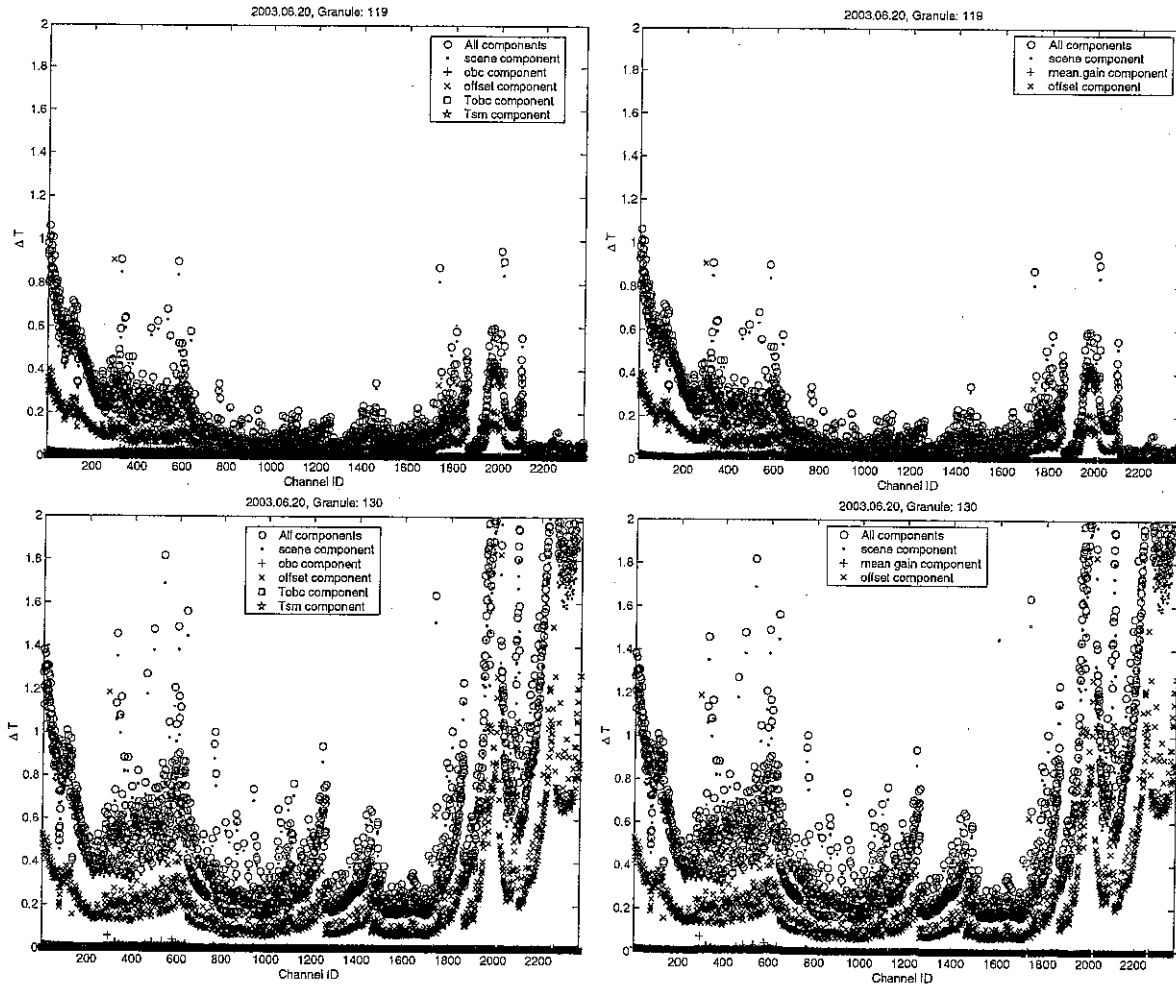


Figure 9. This figure shows the absolute contributions of each of the components to the radiance error. The components calculated from Equation 5 are on the left and the components calculated from Equation 6 are on the right.

6. RADIANCE ERRORS

We calculate the radiance error components where Δn_{sc} is calculated as described in Equation 14. The difference between the total radiance uncertainty calculated by equations 5 and 6 is $\leq 10^{-4}$ K for most channels. The uncertainties calculated from Equation 6 is just slightly larger for some channels because the orbital variation of the gain causes `gain_stats.dev` to be larger than the actual uncertainty of the gain.

Figure 9 shows the absolute radiance errors in temperature units. The uncertainty in the scene counts is the largest contribution to the radiance error. Also, just as was the case for the gains, the contributions to the radiance uncertainty due to the uncertainty in the obc temperature and the scan mirror temperature are negligible. The relative error depends on the scene, however, for a daytime ocean granule the radiance uncertainty is $< 1\%$ more most channels. The uncertainties displayed in Figure 9 are consistent with comparisons of AIRS data with Real-Time Global Sea Surface Temperature measurements.³

We can also compare how good an approximation to the actual noise the NeN is by dividing the NeN by the total radiance uncertainty (Figure 10). For most channels the NeN underestimates the total radiance uncertainty by $\sim 7\%$. This is simply because the NeN is an approximation of the scene component of the total

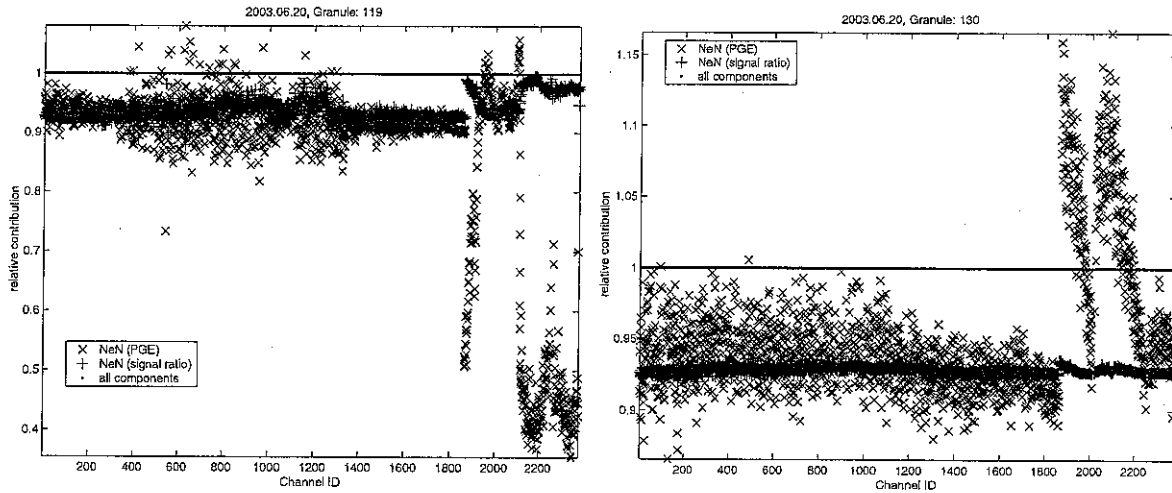


Figure 10. The NeN is divided by the root sum of the squares of all of the contributions to the radiance uncertainty.

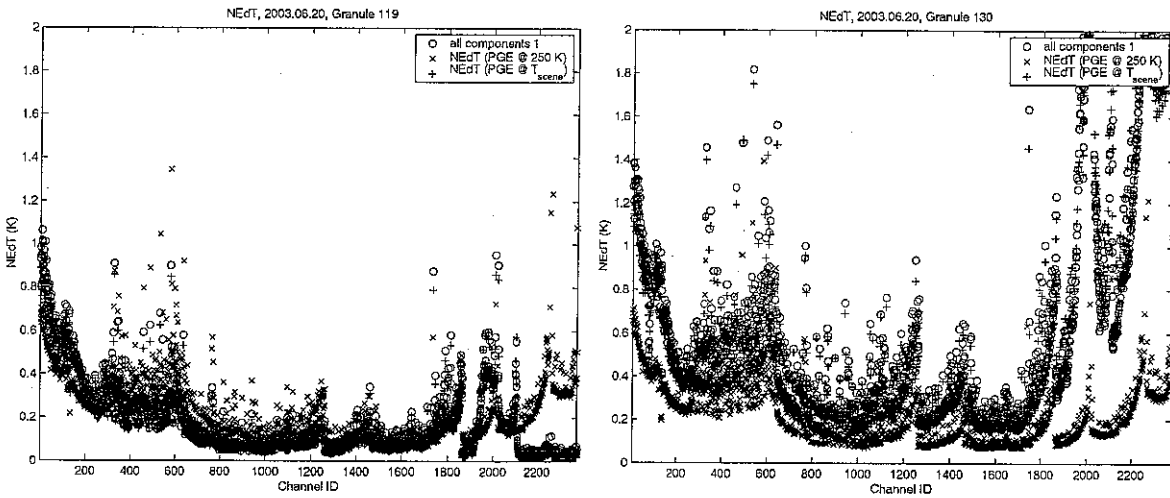


Figure 11. Several methods for calculating the NEdT are compared with the root sum of the squares of all of the radiance error components.

uncertainty of the radiance which neglects the other smaller components. Also, the NeN for a 250 K reference scene underestimates the noise for warm scenes and overestimates the noise for cold scene in Modules 1A, 1B, 2A, and 2B that are the most affected by photon noise.

When the NeN calculated by the PGE is converted to NEdT for a 250 K reference scene it can either overestimate or underestimate the actual NEdT depending on the scene (Figure 11). However, converting the NeN provided by the PGE to an NEdT at the actual scene temperature improves the estimated NEdT significantly.

7. CONCLUSIONS

1. The major component to the radiance uncertainty is the uncertainty in the scene counts.
2. The major component to the gain uncertainty is the uncertainty in the obc counts.

3. The NeN calculated by the level 1B PGE underestimates the radiance uncertainty by $\sim 7\%$ for most channels. If necessary, this could be corrected by adding terms to the NeN equation to account for the uncertainty of the offset and the gain.
4. For channels in Modules 1A, 1B, 2A, and 2B that are the most affected by photon noise, the NeN calculated using the mean scene signal is different than the NeN calculated in the PGE using a 250 K reference temperature. Users should be aware of this difference.
5. The orbital variation of the gain results in small radiance biases at the beginning and ending of granules for some channels. For most channels this contributes to a brightness temperature bias of < 0.01 K. This bias is smaller than the uncertainty of the gain for most channels.
6. After the uncertainty in the scene counts, the space view offset is the largest contributor to the radiance uncertainty. If we implement algorithms to remove all other sources of uncertainty, the uncertainty in the radiances can be improved by at most $\sim 7\%$.
7. These analyses are based on v3.0.5.0 of the AIRS Level 1B algorithms. More recent versions (\geq v3.7.12.x) include an improved offset calculation. The improved offset algorithm results in $Const_{sv} \sim 1.0$ and $Const_{off} \sim 0.17$. Thus, the assumptions made for calculating the NeN in the PGE are better and the uncertainties due to the offset calculation are ~ 0.4 lower than what is reported in this paper.

ACKNOWLEDGMENTS

This work was funded by the AIRS project.

REFERENCES

1. T. S. Pagano, H. H. Aumann, and L. Strow, "Pre-launch performance characteristics of the atmospheric infrared sounder (airs)," *SPIE Proceedings* 4169, p. 41, 2000.
2. T. S. Pagano, H. H. Aumann, D. S. Hagan, and K. Overoye, "Prelaunch and in-flight radiometric calibration of the atmospheric infrared sounder (airs)," *IEEE Transactions on Geoscience and Remote Sensing* 41, pp. 265-273, 2003.
3. H. H. Aumann, M. Chahine, and D. Barron, "Sea surface temperature measurements with airs:rtg.sst comparison," *SPIE Proceedings* 5151, pp. 252-261, 2003.